Electronic Supplementary Material (ESI) for Journal of Materials Chemistry A.

Relationship between surface open cells of α-MnO_2 and CO oxidation ability from a surface focused point of view

Kezhi Li, Jianjun Chen,* Yue Peng, Weichen Lin, Tao Yan, and Junhua Li*

State Key Joint Laboratory of Environment Simulation and Pollution Control, School of Environment, Tsinghua University, Beijing 100084, China

E-mail: chenjianjun@tsinghua.edu.cn; lijunhua@tsinghua.edu.cn

Experimental Details

Infrared analysis (IR). Transmission IR was conducted on an IR spectrometer (Nicolet NEXUS 670, Thermo Fisher). The samples were diluted by dried KBr powders to ensue the transmittance is higher than 20 %.

X-ray diffraction (XRD). XRD was conducted on an X-ray diffractometer (RINT2000, Rigaku Co.). A Cu-target was used as X-ray source with a coupled wavelength of 0.15406 nm and 0.15444 nm, which was post-separated by deconvolution. The X-ray was generated by 40 keV electron with 200 mA current. Step-scan mode was applied with a minimal step of 0.02 ° and 1 s per step. The scan was conducted in the range of 10 - 120 °.

Morphology analysis. Scanning electron microscopy (SEM) was used for a large scale morphology analysis. SEM was conducted on a scanning electron microscope (ProX, Phenom). A CeB_6 source was used to yield electrons. The accelerating voltage was 15 kV. The image was generated by back-scattered electrons (BS).

Other experiments details can be found in the main text.

Models

Reaction Rate Equation

The catalyst is simplified as a one-dimensional uniform cylinder with length of L and crossing area of A. Consider that the oxidation of CO follows pseudo-first-order kinetic model, which can be defined as below:

$$\frac{\mathrm{d}C(x,t)}{\mathrm{d}t} = kC(x,t) \tag{1}$$

where $C(x,t)$ is the concentration at position x and time t, and k is the reaction rate constant.

Due to the gas has a non-zero flow rate, the total differential should be expanded by $\partial C(x,t)/\partial x$, yielding:

$$-\frac{\partial C(x,t)}{\partial x}\frac{\partial x}{\partial t} = kC(x,t) \tag{2}$$

The flow rate $\partial x/\partial t$ equals to F/A, resulting in:

$$-\frac{\partial C(x,t)}{\partial x}\frac{F}{A} = kC(x,t) \tag{3}$$

Since in a steady experiment, concentration is independent of time, which is $C(x,t) = C(x)$. Herein the partial differential equation can be degraded to an ordinary differential equations:

$$-\frac{\mathrm{d}C(x)}{\mathrm{d}x}\frac{F}{A} = kC(x) \tag{4}$$

The solution of this differential equation is:

$$k = -\frac{F}{V}\ln\frac{C_{\mathrm{out}}}{C_{\mathrm{in}}} = -\frac{F}{V}\ln\left(1-X\right) \tag{5}$$

Reaction rate is usually normalised by surface area, which can be defined as:

$$r = -\frac{\mathrm{d}^2 n(x,t)}{\mathrm{d}A\mathrm{d}t} \tag{6}$$

where r is the normalised reaction rate, with a unit of $\mathrm{mol{\cdot}m^{-2}{\cdot}s^{-1}}$, and n is the mole of molecule.

Since $n(x,t)$ is independent of t, then $n(x,t) = n(x)$, which can be expanded by $\mathrm{d}^2 n(x,t) = \mathrm{d}C(x,t)\mathrm{d}V$. And by definition of S_{BET}, $\mathrm{d}A$ can be expanded by $\mathrm{d}A = \rho \mathrm{d}V S_{\mathrm{BET}}$. Herein, the normalised reaction rate r can be written as:

$$r = -\frac{\mathrm{d}C(x,t)}{\rho S_{\mathrm{BET}}\mathrm{d}t} \tag{7}$$

By combining Eq. 1, Eq. 5, and Eq. 7, the final equation can be derived:

$$r = -\frac{1}{S_{\mathrm{BET}}}\frac{F}{m}C_{\mathrm{in}}\ln\left(1-X\right) \tag{8}$$

which is used for calculation in the main text.

Kinetic Models

Before the analysis of the kinetic models, a further explanation for the simplification referred in the manuscript will be first discussed here. In our model as in the main text, the desorption of CO_2 is simplified and all the products related to CO_2 are regarded as CO_2(g) to avoid the appearance of CO_2(ads). The validity of the simplification will be proved if the desorption reaction is considered:

$$CO_2(\mathrm{ads}) \longrightarrow CO_2(\mathrm{g}) \tag{9}$$

where $p_{CO_2}/\theta_{CO_2} = K_{\mathrm{des}}$ since the step is not the rate determine step (RDS). Therefore, θ_{CO_2} is proportional to p_{CO_2} and the scaling relationship is independent to the reaction details.

Herein, θ_{CO_2} can always be replaced by p_{CO_2}/K_{des} in the kinetic analysis. Because we do not concern about the exact number of kinetic parameters in this research, $1/K_{des}$ will be merged into other kinetic parameters (including K_i and k_i). Thus, the simplification to neglect the difference between CO_2(ads) and CO_2(g) is valid.

As is discussed in the main text, the overall reaction path can be written as a combination of the following steps.

$$CO(g) + Mn(suf) \longrightarrow CO(ads){-}Mn(suf) \tag{10}$$

$$CO(ads){-}Mn(suf) + O(latt) \longrightarrow CO_2(g) + Mn(suf) + Vac(O) \tag{11}$$

$$Vac(O) + O_2(g) \longrightarrow O_2(ads) \tag{12}$$

$$CO(ads){-}Mn(suf) + O_2(ads) \longrightarrow CO_2(g) + Mn(suf) + O(latt) \tag{13}$$

To construct the kinetic model, two constraints are included in the calculation. By analysing the whole reaction cycle, it can be observed that CO only adsorbs on Mn-site while the oxygen species are always related to the O-site. Herein, we define the ratio of unoccupied Mn-sites as θ_{Mn}, and the ratio of the Mn-sites with CO(ads) is thus $1 - \theta_{Mn}$. And we also define the ratio of O(latt), Vac(O) and O_2(ads) to be θ_{O-latt}, θ_{O-vac}, and θ_{O-ads}. And the ratios add up to 1, that is:

$$\theta_{O-latt} + \theta_{O-vac} + \theta_{O-ads} = 1 \tag{14}$$

Two cases are considered in the reaction: RDS is the oxidation of CO(ads) by O(latt), which is Eq. 11; another case is that RDS is the oxidation of CO(ads) by O_2(ads), which is Eq. 13.

Case 1: Lattice oxygen determine the reaction rate. Considering the first case, where RDS is Eq. 11, the other steps are considered to reach equivalence. Considering the

equivalence of Eq. 10, an equality can be obtained:

$$\frac{1-\theta_{\mathrm{Mn}}}{p_{\mathrm{CO}}\theta_{\mathrm{Mn}}} = K_1 \tag{15}$$

where p means the relative pressure of the certain gas and K means the equilibrium constant. Thus θ_{Mn} can be calculated as:

$$\theta_{\mathrm{Mn}} = \frac{1}{1+K_1 p_{\mathrm{CO}}} \tag{16}$$

Similarly, by considering Eq. 12 and Eq. 13, two equations can be obtained:

$$\frac{\theta_{\mathrm{O-ads}}}{\theta_{\mathrm{O-vac}} p_{\mathrm{O_2}}} = K_3 \tag{17}$$

$$\frac{p_{\mathrm{CO_2}}\theta_{\mathrm{Mn}}\theta_{\mathrm{O-latt}}}{(1-\theta_{\mathrm{Mn}})\theta_{\mathrm{O-ads}}} = K_4 \tag{18}$$

The combination of Eq. 14, Eq. 17, and Eq. 18 can generate the expression of $\theta_{\mathrm{O-latt}}$:

$$\theta_{\mathrm{O-latt}} = \frac{1}{1+\frac{1}{K_1K_4}\frac{p_{\mathrm{CO_2}}}{p_{\mathrm{CO}}}+\frac{1}{K_1K_4}\frac{1}{K_3 p_{\mathrm{O_2}}}\frac{p_{\mathrm{CO_2}}}{p_{\mathrm{CO}}}} \tag{19}$$

The reaction rate can be obtained by the RDS which is Eq. 11. That is:

$$r = \frac{\mathrm{d}p_{\mathrm{CO_2}}}{\mathrm{d}t} = k_2(1-\theta_{\mathrm{Mn}})\theta_{\mathrm{O-latt}} \tag{20}$$

By substituting the variables from Eq. 16 and Eq. 19, the reaction rate can be expressed as:

$$r = k_2\frac{1}{1+\frac{1}{K_1 p_{\mathrm{CO}}}}\frac{1}{1+\frac{1}{K_1K_4}\frac{p_{\mathrm{CO_2}}}{p_{\mathrm{CO}}}+\frac{1}{K_1K_4}\frac{1}{K_3 p_{\mathrm{O_2}}}\frac{p_{\mathrm{CO_2}}}{p_{\mathrm{CO}}}} \tag{21}$$

If we define $\gamma = \frac{p_{\mathrm{CO_2}}}{p_{\mathrm{CO}}}$, then the equation can be simplified as:

$$r = k_2\frac{1}{1+\frac{1}{K_1 p_{\mathrm{CO}}}}\frac{1}{1+\frac{1}{K_1K_4}\gamma+\frac{1}{K_1K_3K_4}\frac{\gamma}{p_{\mathrm{O_2}}}} \tag{22}$$

or as another form:

$$\frac{k_2}{r(1+\frac{1}{K_1 p_{\mathrm{CO}}})} = 1 + \frac{1}{K_1 K_4}\gamma + \frac{1}{K_1 K_3 K_4}\frac{\gamma}{p_{\mathrm{O_2}}} \tag{23}$$

Case 2: Adsorbed oxygen determine the reaction rate. In this case, the difference is that the RDS is the oxidation of CO(ads) by O_2(ads), which is Eq. 13. The analysis is similar, while in this case, the reaction Eq. 11 reaches the equilibrium:

$$\frac{p_{\mathrm{CO_2}}\theta_{\mathrm{Mn}}\theta_{\mathrm{O-vac}}}{(1-\theta_{\mathrm{Mn}})\theta_{\mathrm{O-lat}}} = K_2 \tag{24}$$

Hence, by combining Eq. 14, Eq. 17, and Eq. 24, $\theta_{\mathrm{O-ads}}$ can be calculated as:

$$\theta_{\mathrm{O-ads}} = \frac{1}{1 + \frac{1}{K_3 p_{\mathrm{O_2}}} + \frac{1}{K_1 K_2}\frac{p_{\mathrm{CO_2}}}{p_{\mathrm{CO}}}\frac{1}{K_3 p_{\mathrm{O_2}}}} \tag{25}$$

By analysing Eq. 13 as the RDS, the rate can be written as:

$$r = k_4 \frac{1}{1+\frac{1}{K_1 p_{\mathrm{CO}}}} \frac{1}{1 + \frac{1}{K_3 p_{\mathrm{O_2}}} + \frac{1}{K_1 K_2}\frac{p_{\mathrm{CO_2}}}{p_{\mathrm{CO}}}\frac{1}{K_3 p_{\mathrm{O_2}}}} \tag{26}$$

or can be simplified as:

$$r = k_4 \frac{1}{1+\frac{1}{K_1 p_{\mathrm{CO}}}} \frac{1}{1 + \frac{1}{K_3}\frac{1}{p_{\mathrm{O_2}}} + \frac{1}{K_1 K_2 K_3}\frac{\gamma}{p_{\mathrm{O_2}}}} \tag{27}$$

or as another form:

$$\frac{k_4}{r(1+\frac{1}{K_1 p_{\mathrm{CO}}})} = 1 + \frac{1}{K_3}\frac{1}{p_{\mathrm{O_2}}} + \frac{1}{K_1 K_2 K_3}\frac{\gamma}{p_{\mathrm{O_2}}} \tag{28}$$

Crystal Structure

The structure of $\alpha-\mathrm{MnO_2}$ and $\beta-\mathrm{MnO_2}$ is further discussed here in this section as in Figure S1 and S2. Though belonging to different phases, both MnO_2 constitute of similar [MnO_6] units as in Figure S1(a) and S2(a). The similar skeleton structure is the base for

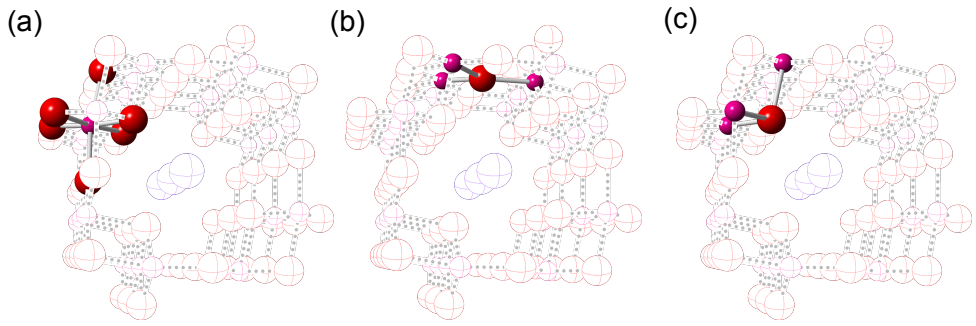

Figure S 1: Structure of $\alpha-MnO_2$. (a)[MnO_6] octahedra. (b)sp^2-hybridised of O. (c)sp^3-hybridised of O. Pink: Mn; Red: O; Purple: K.

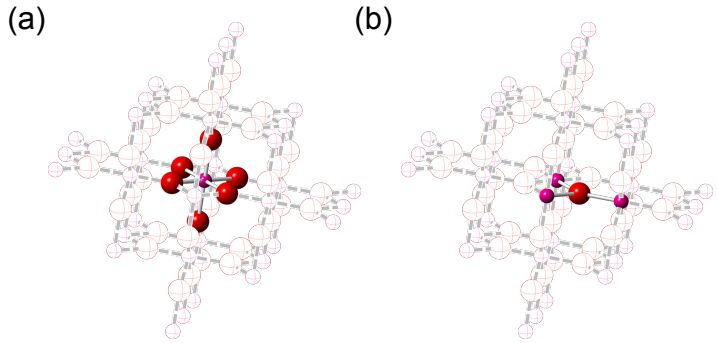

Figure S 2: Structure of $\beta-MnO_2$. (a)[MnO_6] octahedra. (b)sp^3-hybridised of O. Pink: Mn; Red: O.

the comparison between α- and $\beta-MnO_2$. However, the hybridization is different for α- and $\beta-MnO_2$. In $\alpha-MnO_2$, both sp^2 and sp^3 hybridization exist for O, while only sp^2-hybridised O can be observed in $\beta-MnO_2$ as in Figure S1(b)(c) and S2(b).

Part of the models are visualised by using the QuteMol packages.[1]

TEM Simulation

As is shown in Figure S3, HRTEM is formed by the interaction of electrons with the atom columns in the materials. Unlike the commonly observed depth contrast in TEM, the image is formed owing to the difference of phase contrast. Therefore, the interpretation of HRTEM is usually highly relied on TEM simulation.

In our experiment, the dark dots correspond to tunnels of $\alpha-MnO_2$, while the white

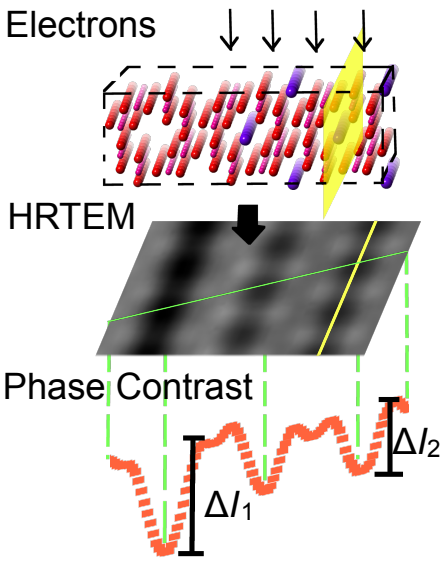

Figure S 3: Scheme for the formation of phase contrast in the HRTEM.

dots related to the skeletal Mn-O columns. The phase contrast of the two area are denoted as I_{tunnel} and I_{skeleton} respectively. Since the crystal is periodically repeated by tunnels and skeleton area, there are cycling dark fringes and bright fringes observed in HRTEM, and correspondingly, there are troughs and crests in phase contrast presentation. Above is the basic interpretation of the HRTEM and phase contrast.

Since phase contrast is sensitive to the element constitution in the atom columns, if K^+ cations are depleted from the tunnels, there will be a difference in phase contrast. To simplify the analysis, phase contrast difference is focused in the research which is defined as $\Delta I = I_{\text{skeleton}} - I_{\text{tunnel}}$, as shown in Figure S3. Based on the simulation, two cases are considered to account for the HRTEM as in Figure S3: (1) if K^+ cations are totally depleted from the tunnels, a relatively large phase contrast difference ΔI_1 is expected; (2) if K^+ cations fully occupy the tunnels, a relatively small phase contrast difference ΔI_2 is expected. Thus, phase contrast difference ΔI is used in our research to analyse the tunnel occupation status of $\alpha-MnO_2$.

Results

Physical Characterisation

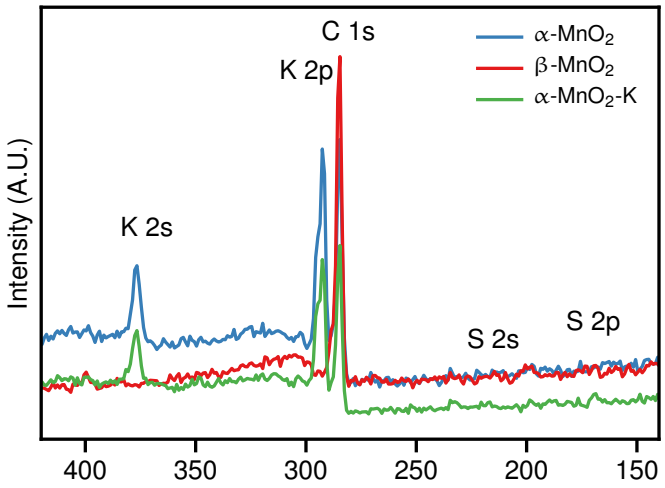

Figure S 4: XPS scanning results of the samples.

To analyse the remaining elements at the surface of the samples, XPS is used due to its high sensitivity to the surface elements, which is shown in Figure S4. All samples except $\beta-MnO_2$ contain a small amount of surface K which is a typical feature for $\alpha-MnO_2$. However, there is no signal at 295 and 377 eV (corresponding to K 2p and 2s respectively), proving that there is no detectable S remained at the surface of the samples.

To confirm that no $HCOO^-$ remains at the surface of $\alpha-MnO_2-K$, IR spectra were obtained for $\alpha-MnO_2$ and $\alpha-MnO_2-K$ as in Figure S5. The characteristic pattern for $HCOO^-$ at 1600 - 1500 cm^{-1} or any pattern for carbonyl groups at 1900 - 1500 cm^{-1} are not observed for $\alpha-MnO_2$ or $\alpha-MnO_2-K$. The only observable peaks at around 720, 585, 522, 465 cm^{-1}, and a peak around 400 cm^{-1} are typical pattern for $\alpha-MnO_2$.[2]

The crystal structure of the samples is proved to be α- and β-MnO_2 as in XRD in Figure S6. No extra diffraction peaks are observed, confirming the purity of the samples. $\alpha-MnO_2-K$ is also confirmed to be like $\alpha-MnO_2$, without any impurities detected. The intensity difference between α-MnO_2 sample and the standard card is due to the fact that

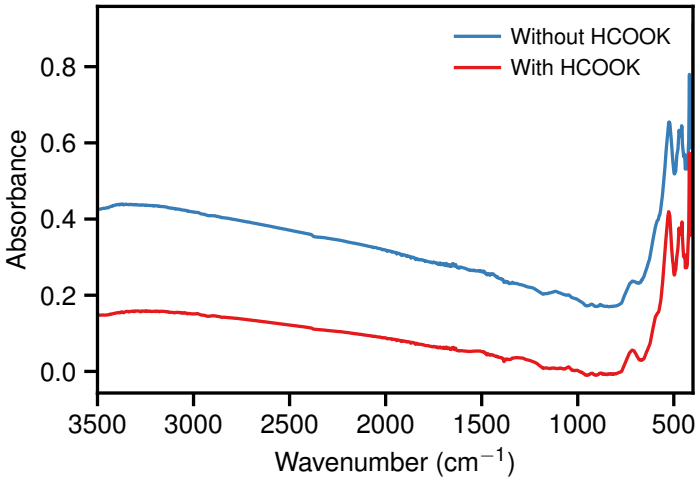

Figure S 5: IR of $\alpha-MnO_2$ and $\alpha-MnO_2-K$.

the concentration of K^+ is strongly dependent on synthesis, which will influence the XRD intensity but not the position of the peaks.

The general morphology of α- and β-MnO_2 are shown in Figure S7. Both samples share the similar rod-like structure, with a length of a few micrometers.

N_2 adsorption-desorption isotherm for samples are displayed in Figure S8. The isotherm for α-MnO_2 belongs to Type-IV in classification which typically has a hysteresis loop, indicating the existence of mesopores. The relatively higher amount of adsorbed N_2 indicates a higher specific area, which was calculated by BET equation in the main text.

CH_3OH Probe Experiments

In situ-FTIR of CH_3OH probe adsorption experiment results are shown in Figure S9. Three peaks can be observed in the range from 1800 cm^{-1} to 950 cm^{-1}. The coupled peaks at around 1600 cm^{-1} and 1400 cm^{-1} are ascribed to the asymmetric and symmetric vibration of carboxylic ion (-COO^-), respectively, while the peak around 1050 cm^{-1} is ascribed to -C-O vibration. The former belongs to the oxidation products of CH_3OH such as $HCOO^-$, while the latter belongs to the species adsorbed on acid sites. The classification is in agreement with Tatibouët's previous work.[3] There are two negative peaks observed in β-CeO_2 at around

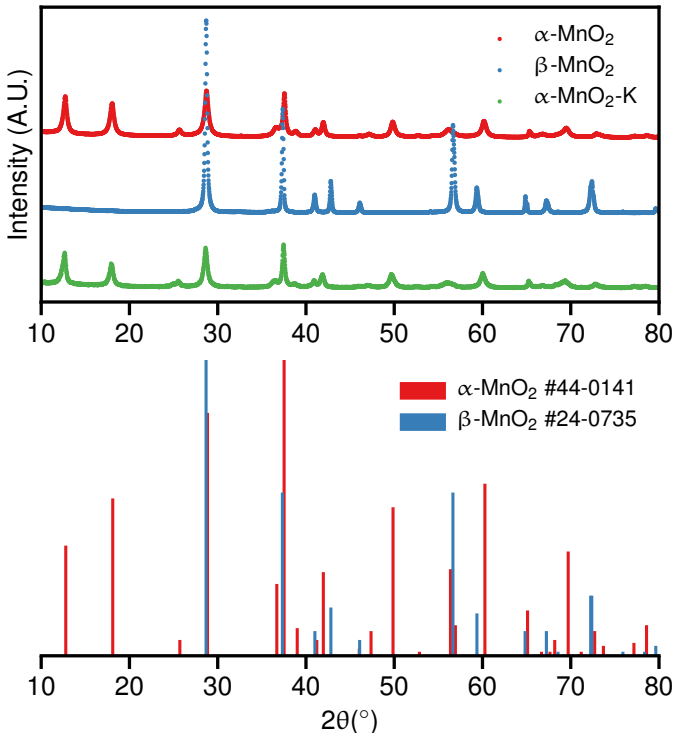

Figure S 6: XRD of α-, β-MnO_2 and $\alpha-MnO_2-K$. The lower figure displays the standard XRD pattern.

1350 cm^{-1} and 1180 cm^{-1}, which are tentatively ascribed to the lattice vibration of β-MnO_2 in agreement with previous literature.[4,5] Since the adsorption amount of CH_3OH is rather low, it is reasonable that the signal of adsorbates is weak compared with the intensity change of the adsorbents. CH_3OH adsorption gradually reaches stability after around 60 min for both samples as in Figure S9(b)(d).

By inspecting the spectra at the last spectrum of the experiment, it can be observed that a large ratio of CH_3OH is oxidised on the surface of α-MnO_2 compared with β-MnO_2. Though the signal for $\alpha-MnO_2-K$ is relatively weak, the intensity for $-COO^-$ is still higher than $-C-O$, having the similar pattern with $\alpha-MnO_2$. It suggests that K^+ cations are blocking substances but do not change the surface property of MnO_2. The time-dependent integration result is shown and explained in the main text.

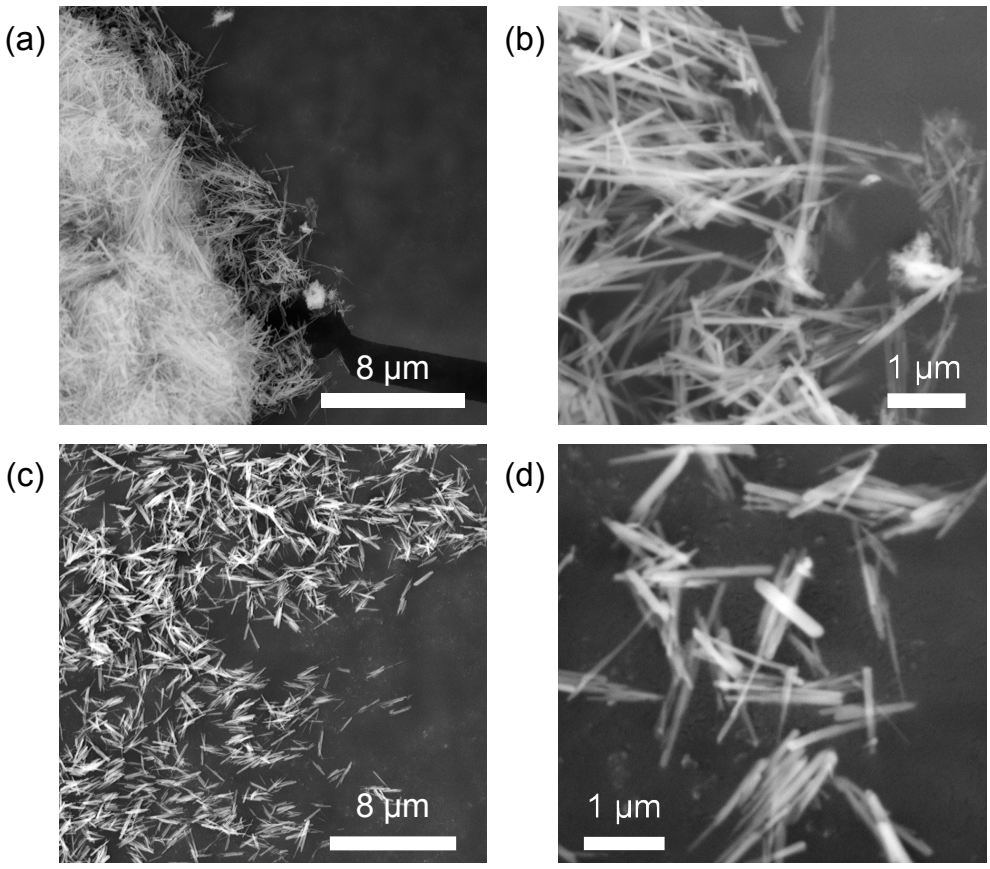

Figure S 7: SEM of (a-b) α-MnO_2 and (c-d) β-MnO_2.

Mn Valence Analysis by XPS

Mn valence was analysed by XPS. Mn 3s spectra were used for analysis rather than 2p spectra due to the overlap of different valences in 2p spectra. The valence analysis was based on the linear relationship between the splitting of Mn 3s spectra and its valence as reported before.[6] The obtained spectra were shown in Figure S10. The quantification and analysis can be referred in the main text.

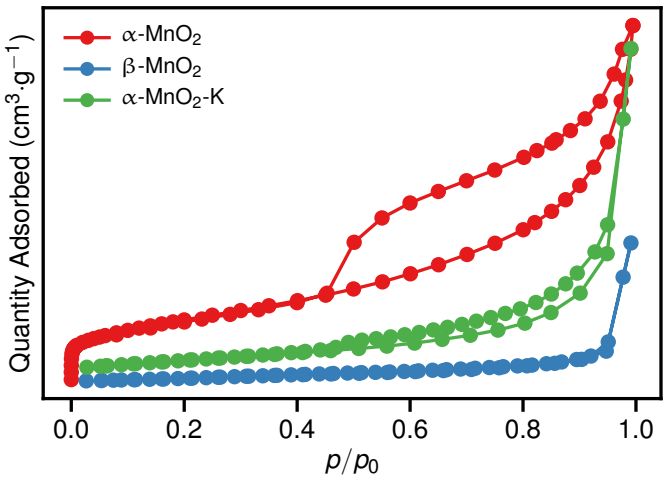

Figure S 8: N_2 adsorption-desorption isotherm for α-, β-MnO_2 and $\alpha-MnO_2-K$.

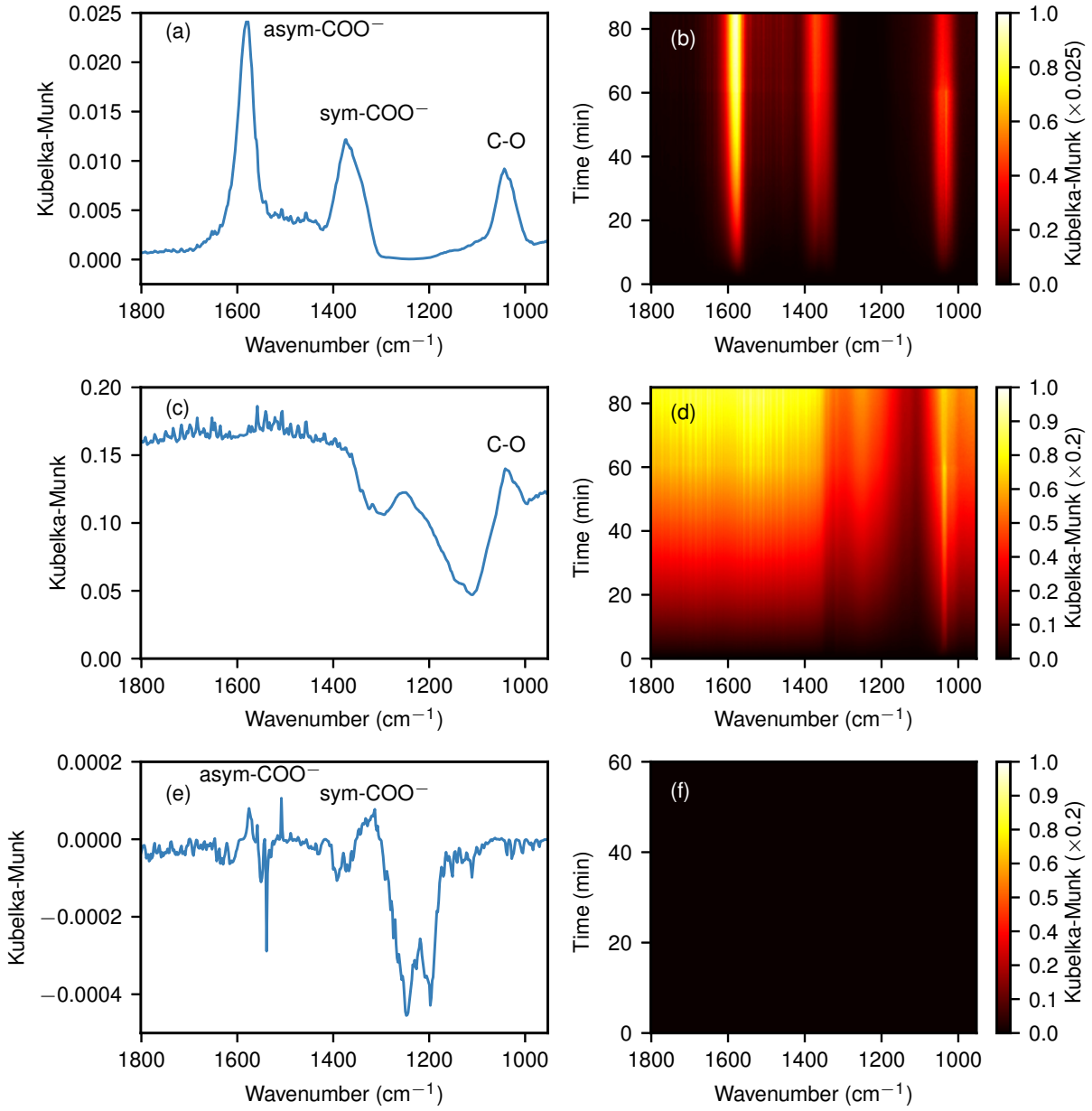

Figure S 9: In situ-FTIR of CH_3OH probe adsorption on the surface of (a)(b) α-MnO_2, (c)(d) β-MnO_2 and (e)(f) $\alpha-MnO_2-K$. (a)(c)(e) The last IR spectrum of the adsorption experiment for α-MnO_2, β-MnO_2 and $\alpha-MnO_2-K$, respectively. (b)(d)(f) Absorption signal against wavenumber and adsorption time.

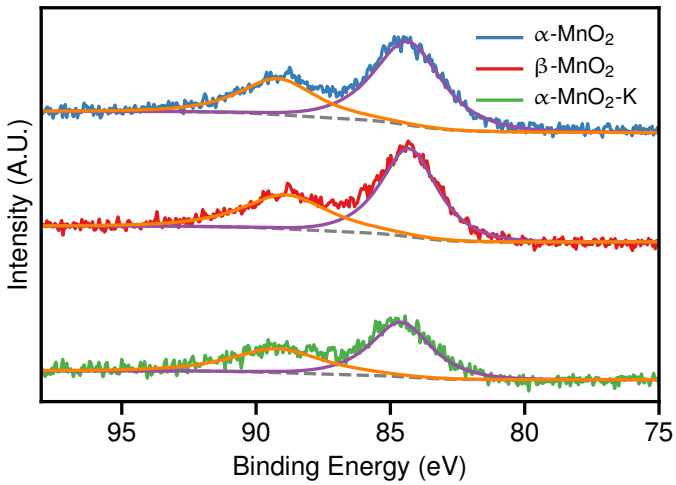

Figure S 10: Mn 3s spectra for α-MnO_2, β-MnO_2 and $\alpha-MnO_2-K$, respectively.

References

(1) Tarini, M.; Cignoni, P.; Montani, C. *IEEE T. Vis. Comput. Gr.* **2006**, *12*, 1237–1244.

(2) Julien, C.; Massot, M.; Poinsignon, C. *Spectrochim. Acta, Part A* **2004**, *60*, 689 – 700.

(3) Tatibouët, J. *Appl. Catal., A* **1997**, *148*, 213 – 252.

(4) Ma, H.; Shen, J.; Shi, M.; Yan, B.; Li, N.; Ye, M. *Mater. Res. Bull.* **2011**, *46*, 1461 – 1466.

(5) Tang, N.; Tian, X.; Yang, C.; Pi, Z.; Han, Q. *J. Phys. Chem. Solids* **2010**, *71*, 258 – 262.

(6) Galakhov, V. R.; Demeter, M.; Bartkowski, S.; Neumann, M.; Ovechkina, N. A.; Kurmaev, E. Z.; Lobachevskaya, N. I.; Mukovskii, Y. M.; Mitchell, J.; Ederer, D. L. *Phys. Rev. B* **2002**, *65*, 113102.